Electrochimica Acta 188 (2016) 710–717

Contents lists available at ScienceDirect

Electrochimica Acta

journal homepage: www.elsevier.com/locate/electacta

Effect of the electrophoretic deposition of Au NPs in the performance CdS QDs sensitized solar Cells

I. Zarazúa[a,c], D. Esparza[a], T. López-Luke[a], A. Ceja-Fdez[a], J. Reyes-Gomez[b], I. Mora-Seró[c], E. de la Rosa[a,*]

[a] Centro de Investigaciones en Óptica, A.P. 1-948 León, Gto. 37150, Mexico
[b] Facultad de Ciencias, Universidad de Colima, Colima Col. 28045, Mexico
[c] Institute of Advanced Materials, Universitat Jaume I, 12071 Castelló, Spain

ARTICLE INFO

Article history:
Received 8 July 2015
Received in revised form 19 November 2015
Accepted 25 November 2015
Available online 27 November 2015

Keywords:
Solar Cells
Quantum dots
Impedance spectroscopy
Au Nanoparticles

ABSTRACT

Solution-processed mesoscopic oxide semiconductor-based materials offer potentially low-cost and high stability alternative for next generation of solar cells, and metallic nanoparticles had shown to be a good alternative to improve specific parameters in such kind of devices. In the present work, it is showed the systematic study of the effect of electrophoretic gold nanospheres (Au NPs) with cadmium sulfide Quantum Dots (CdS QDs) sensitized TiO_2 solar cells. Au NPs were added by electrophoretic deposition at several times (0.5, 2.5 and 7.5 minutes) and CdS QDs were deposited by a Successive Ionic Layer Absorption and Reaction (SILAR) method. Electrophoretic deposition allowed to significantly decrease the Au NPs deposition times respect previously reported methods. The results show that Au NPs reduce the photocurrent (from 9.85 to 9.44 mA/cm^2) at the same time that increase the open circuit voltage (V_{oc}) (from 575 to 618 mV) and the Fill Factor (FF) (from 46 to 51%) which result in a final increase of the photoconversion efficiency (η) (from 2.63 to 2.96% for 0.5 min of deposit). A systematic characterization permitted to identify the origin of the variations observed in the solar cell parameters with and without Au NPs. Incident Photon to Current conversion efficiency (IPCE) demonstrate that the Au NPs reduces the amount of light that reach the CdS QDs and Impedance Spectroscopy (IS) analysis, indicates a downshift in the TiO_2 conduction band (CB) and decreases the recombination processes, resulting in the observed increase in the FF and V_{oc}.

1. Introduction

Nanomaterials have emerged as a new and promising alternative for harvesting solar energy [1–7]. The use of nanomaterials for solar cells could reduce production costs due to the low synthesis temperature and deposition methods [1], although the photoconversion efficiency for such devices is still generally much lower than that of the best silicon-based solar cells (η=25%) [8]. The advantages of nanostructured solar cells include the possibility to manipulate factors such as shape and size of the particles to improve the conversion efficiency, making them commercially feasible [9–12]. One key factor to increase conversion efficiency is to improve both electron and hole mobility to avoid recombination. One of the most studied hybrid-type nanostructured solar cells is the Grätzel or dye sensitized solar cell (DSSC) [11,13–16]. DSSCs typically consist of TiO_2 NCs acting as a highly porous, wide band gap semiconductor for electron collection, and dye molecules adsorbed onto the TiO_2 NCs surface acting as sensitizers to harvest solar light. The largest photoconversion efficiency of DSSC reported in literature is 12%, obtained with a ruthenium-based dye [16,17]. Unfortunately, this type of solar cell is expensive because of the high cost of the dye.

Quantum dots (QDs), *e.g.*, CdSe, CdTe, CdS, PbS, PbSe, Bi_2S_3, and InP [12,15,18–21], have been studied as an alternative to ruthenium dyes in DSSC to reduce costs and increase efficiency. QDs have large extinction coefficients in the visible region and, after bandgap excitation, undergo charge separation, injecting electrons to the conduction band of the metal oxide [22]. Therefore, it is possible to increase the driven force for electron transfer by controlling the crystallite size of QDs, which in turn can improve the conversion efficiency [23].

* Corresponding author. Fax: +52 477 441 42 09.
E-mail address: elder@cio.mx (E. de la Rosa).

http://dx.doi.org/10.1016/j.electacta.2015.11.127
0013-4686/

The photoresponse of semiconductors has also been improved with the presence of metallic NPs such as gold (Au) and silver (Ag), although the mechanism of the observed enhancement is not completely understood [9–12,24–26]. It has been suggested that such NPs enhance the visible-light-induced electron-transfer process via Surface plasmon resonance [11,13–16]. However, mechanistic evidence that directly supports electron transfer arising from plasmon excitation remains elusive.[10,11,16,17,27,28]. Enhancement of photoconversion efficiency has also been reported in Si thin films in the presence of Au NPs. In this case, the proposed mechanism was based on the absorption enhancement of Si thin film via the excitation of the surface plasmon resonance (SPR) [16,17,29,30]. However, for larger particle sizes, the dominant mechanism is based on the increment of light scattering and absorption of the Si-thin film [12,15,18–21,31–33]. Similarly, a strong increase in photoconversion efficiency with QD-sensitized Au-TiO_2 NP composite have been found which was attributed to enhanced absorption of QDs caused by increased scattering of light by the Au NPs [24]. Other authors, had found that Au NPs act as electron traps to help separate the photogenerated charges and subsequently improve interfacial charge transfer [21,25,26,34,35]. Studies also have shown a shift in the Fermi level to a more negative level (in respect to vacuum) by doping the semiconductor with metal NPs. This shift enhances the efficiency of the interfacial charge transfer process [36]. Alternatively, metallic NPs have been suggested to act as sensitizers in TiO_2 NCs and zinc oxide (ZnO) nanowires, similar to organic dyes, based on the photo- response and the absorption spectra of metallic NPs [26,37]. In such a case, the electron injection from Au NPs to TiO_2 competes effectively with electron relaxation within Au NPs.

In this work, we report a systematic characterization of CdS QDs sensitized TiO_2 films decorated with Au NPs at different times of electrophoretic deposition. The objective is to improve the overall photoconversion efficiency by extracting more efficiently the electrons from the QDs with the help of Au NPs. A detailed study of the structural, optical, and photoelectrochemical properties was carried out to gain new insight into the underlying mechanism. Impedance analyses indicate that Au NPs deposited by this method affect at the same time two parameters, reducing the recombination processes and downshifting position of the TiO_2's CB, which result in an increase of the Voc, the electron transport and consequently the FF and η.

2. Experimental

2.1. Preparation of TiO_2 sensitized films

2.1.1. Materials

TiO_2 Paste (WER2-0 Reflector) and TiO_2 Paste (DSL 18NR-T) were obtained from DYESOL, Titanium (IV) isopropoxide (97%), Acetylacetone (>99%), Cadmium acetate dehydrate (Cd $(CH_3COO)_2{\cdot}2H_2O$), Zinc acetate dihydrate ($Zn(CH_3COO)_2{\cdot}2H_2O$) and Sodium hydroxide (NaOH) were obtained from Sigma-Aldrich. Sulphur (S), and Sodium sulphide ($Na_2S{\cdot}9H_2O$) were obtained from KARAL and Fluorine-doped tin oxide (FTO) TEC-15 by MTI.

2.1.2. TiO_2 film Preparation

Fluorine-doped tin oxide (FTO) glasses were cleaned with water, acetone and ethanol in an ultrasonic bath for 15 min each before use. All the photoelectrodes were made of three different TiO_2 layers stacked one on the top of the other. 1) Compact layer: A solution of titanium (IV) Isopropoxide (0.2 M) in acetylacetone/ethanol (1:1 V:V) deposited by spray pyrolysis over an FTO and sintered at 450 °C for 30 min to obtain a 190 nm layer. This layer will avoid shortcuts reducing the recombination processes between the electrolyte and the FTO. 2) Transparent layer: TiO_2 paste, (DSL 18-NRT, 20 nm average particle size) is deposited over the compact layer by Doctor Blade method obtaining a 6 μm thick film. This layer will be the active layer i. e. where the sensitizers will be adsorbed and the mayor of the photo absorption process will be done. And 3) Scattering layer: a 9 μm layer is obtained by doctor blading depositing Wer2-O Reflector paste (400 nm particle size). This last layer will scatter the light that has passed through the first two layers without been absorbed, giving a second chance to be absorbed by the QDs. [15,38–40] In the case of samples for Electron microscopy the scattering layer was omitted to compare de TiO_2 particles of the mesopourus layer with the deposited nanoparticles. The films were sintered for 30 min at 450 °C to obtain a good electrical contact between nanoparticles.

2.1.3. Au nanoparticles synthesis

The synthesis of Au NPs was based on the Turkevich method, by adding 3.75 ml of 1%wt. sodium citrate solution to a 0.001 M $HAuCl_4$ boiling solution and stirring at 500 rpm, until ruby red solution. Then the solution was cooled to room temperature and filtered. With this procedure13 nm particles were obtained. The size and shape were verified via UV–vis absorption spectroscopy and TEM.

2.1.4. Au deposit

After synthesis, the Au NPs were deposited on the TiO_2 films by electrophoresis. The samples were placed face to face with an FTO at distance of 0.2 cm and inserted in a cuvette with 2.5 mL of a colloidal suspension of the corresponding Au nanoparticles. Next, a 5 V DC voltage was applied between the TiO_2 films for several deposition times.

2.1.5. Film sensitization

The TiO_2/Au Nps electrodes were in situ sensitized with CdS QDs grown by SILAR. For this purpose, solutions of 0.05 M Cd $(CH_3COO)_2$ dissolved in ethanol as Cd^{2+} source and 0.05 M Na_2S in methanol:water (V:V = 1:1) as S^{2-} source, were used. A single SILAR cycle consisted of 1 min dip-coating the TiO_2 electrode into the cadmium solution (Cd^{2+}) and subsequently into the sulfide solutions, also during 1 min. After each dipping step in a precursor solution, the electrodes were thoroughly rinsed by immersion in the corresponding solvent in order to remove the excess of precursor. Seven SILAR cycles were done to obtain a uniform coverage of the TiO_2 NPs with CdS QDs. To enhance the photovoltaic performance ZnS is deposited by SILAR for passivate CdS surface and reduce the recombination of electrons in the TiO_2 to the polysulfide electrolyte [21,25,26,34,35,41–43]. ZnS passivation was obtained by using 0.1 M of $Zn(CH_3COO)_2{\cdot}2H_2O$ and 0.1 M of Na_2S both dissolved in water as Zn^{2+} and S^{2-} sources respectively. The films were dipped for 1 min/dip in the solutions during 2 SILAR cycles.

2.1.6. Counter electrode manufacturing and assembling of solar cells

Cu_2S counter electrodes were fabricated by immersing brass foil in an HCl solution (38% by volume) at 90 °C for 1 hour. These substrates were sulfated by adding a drop of poly- sulfide electrolyte solution made by mixing solutions of Na_2S (1 M), S (1.0 M), and NaOH (0.1 M) in distilled water. The solar cells were constructed by assembling the Cu_2S counter electrode and the sensitized TiO_2 film electrode with a binder clip separated by a scotch spacer. Lastly, a polysulfide electrolyte was introduced by dropping into the solar cell.

2.2. Characterization

Transmission Electron Microscopy (TEM) images were obtained from a FEI- Titan 80-300 KeV, microscope, equipped with ultra-

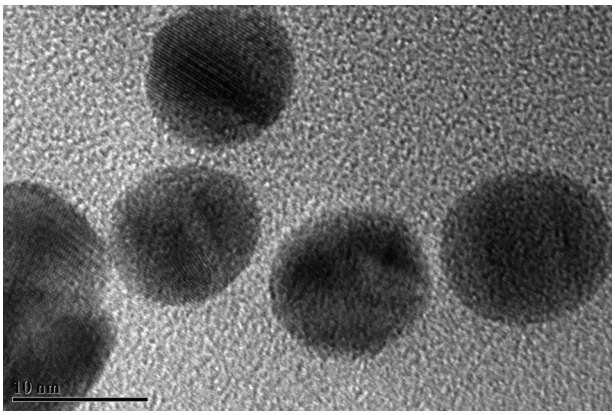

Fig. 1. TEM image of Au nanostructured particle used to decorate the TiO_2 films.

stable Schottky field emitter gun. The UV–vis absorption spectra of the colloidal Au NPs were measured by transmittance and substrates were measured by diffuse reflectance in the range of 360 nm to 800 nm using an Agilent Technologies Cary Series UV-Vis-NIR spectrophotometer (Cary 5000) and an integrating sphere of 60 mm. The current density curves were measured with a reference 600 Gamry potensiotat, scanning from 0 to 600 mV at 100 mV/S. The samples were illuminated with an Oriel Sol 3A solar simulator while measuring. The light intensity was adjusted employing a NREL calibrated Si solar cell having KG-2 filter for one sun light intensity (100 mW/cm^2). Best results are reported. IPCE spectra measurements were made with a monochromator (Newport model 74125). Electrochemical Impendance Spectroscopy (EIS) measurements were carried out by applying a small voltage perturbation (10 mV) at frequencies from 100 Hz to 0.1 Hz for different forward bias voltages in dark conditions.

3. Results

3.1. Structural and Morphological Characterization

3.1.1. Au Nanostructured particles

The representative electron microscopy images from the gold nanostructured particles are shown in Fig. 1. Nanospheres (NPs) have typically 12 nm of diameter and have good size confinement

3.1.2. TiO_2 films

In Fig. 2 are presented SEM images of the transparent layer of the TiO_2 films. It can be seen that when not decorated (Fig. 2 a) the films are composed for 35 nm average size TiO_2 NPs agglomerated

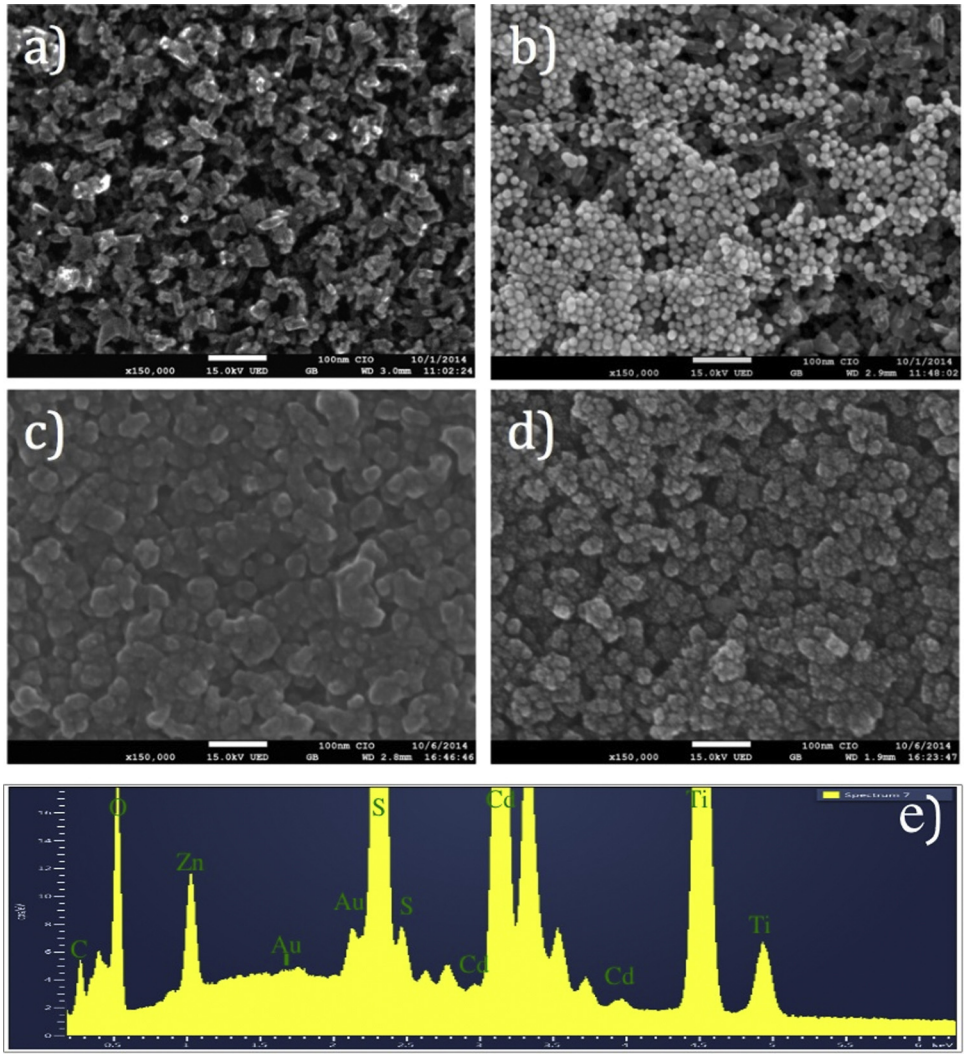

Fig. 2. Representative SEM micrographs of the transparent layer of a) TiO_2 films, b) TiO_2 decorated with Au NPs, c) CdS sensitized TiO_2 by SILAR, d) TiO_2 decorated with Au NPs and sensitized with CdS QDs and e) EDS spectrum of the TiO_2/Au/CdS films showing the principal peaks of Au, Cd and S.

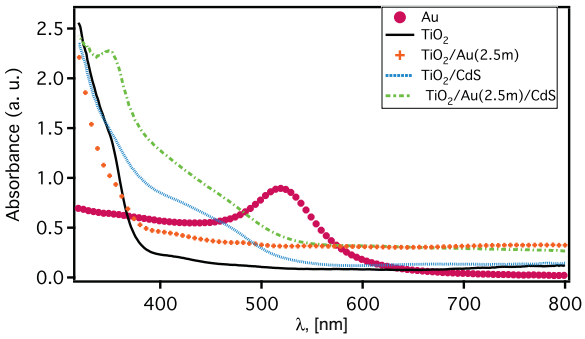

Fig. 3. Representative absorption spectra of TiO_2 films decorated with Au NPs and sensitized with CdS QDs. Showing the spectra of colloidal Au NPs.

in a homogenous high porous arrangement. When Au NPs are electrophoretic deposited (see Fig. 2 b), spherical particles of approximately 13 nm are observed on the film indifferently of the polarity applied to the sample during the deposit. The size and shape of the nanoparticles indicate that they are Au NPs. Here also can be seen that the TiO2 NPs are not modified by the electrophoresis. When the films are SILAR sensitized the TiO_2 NPs are completely covered by the CdS QDs, partially filling the spaces between the particles. This gives the films a soft and less porous appearance (see Fig. 2 c). Finally, when the films are decorated with Au NPs and sensitized with CdS to form TiO_2/Au/CdS samples (Fig. 2 d), a uniform coverage of the film with the QDs is obtained. But the appearance of the deposit is gnarled due to the presence of the Au NPs. EDS analyses of the films (Fig. 2 e) confirm the presence of the Au NPs and Cd and S from the QDs.

3.1.3. Optical Absorption

The absorption spectra of the Au NPs, bare TiO_2 films, CdS QDs sensitized TiO_2 films, 2.5 minutes Au NPs electrophoretic decorated films, Au decorated/CdS QDs sensitized TiO_2 films are shown in Fig. 3. The Au NPs absorption (red circles) presents a well-defined peak at 519 nm that is consistent with the surface plasmon resonance (SPR) for such size of NPs. The TiO_2 films (black solid line) have almost no absorption in the visible region, rapidly increasing for wavelengths (λ) lower than 400 nm. When Au NPs deposit is done for 2.5 min (orange +) there is a uniform increase in the absorption between 380 and 800 nm, pointing to a light scattering effect. While, CdS sensitization of the TiO_2 films (blue doted line) produces an absorption shoulder from 400 to 500 nm, which corresponds to the absorption of the CdS QDs[36,41,44]. Finally, when CdS sensitization is done in 2.5 min Au NPs decorated films, the shape in obtained spectra is similar to the films only sensitized with CdS QDs. But have a general increase in the absorption in the visible region, this increase match with the increase obtained in samples only decorated with Au NPs (orange +).

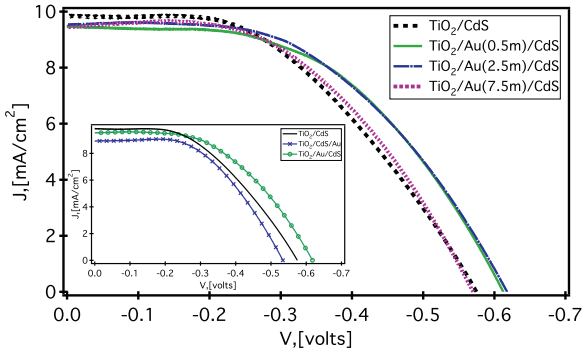

Fig. 4. Representative J–V curves of TiO_2/Au/CdS solar cells at several Au deposition times. Inset showing champion cells of TiO_2/Au/CdS and TiO_2/CdS/Au configuration.

3.2. Photoelectrical Conversion Measurements

3.2.1. J-V Curves

Fig. 4 shows the current density-voltage (J-V) profiles of the TiO_2 films decorated by electrophoresis with Au NPs and further sensitized with CdS QDs (TiO_2/Au/CdS) at several deposition times. Fill Factor (FF) and photoelectrical conversion efficiency (η) were calculated using Eq. 1 and Eq. 2 for short-circuit current density (J_{sc}) and open-circuit voltage (V_{oc}) obtained from the curves [2,24–26,44–46]

$$FF = \frac{P_m}{J_{sc} x V_{oc}} x100 \quad (1)$$

$$\eta = \frac{P_m}{P_i} x100 = FF\frac{J_{sc} x V_{oc}}{P_i} \quad (2)$$

where, P_m is the maximum power (J × V product) observed from the current density-voltage curve for each device and P_i is the incident light power density (100 mW × cm^{-2}). Four samples of each configuration were measured, finding a maximum relative standard deviation of 1.8%. Champion values are listed in Table 1.

Analyzing the curves, it can be seen than the TiO_2/CdS films (black line), have a J_{sc} of 9.85 mA/cm^2 an V_{oc} of 575 mV, a FF of 46.5% and a photoconversion efficiency of 2.63%, which is in good agreement with the efficiencies reported for this kind of solar cells [24–26,47–50]. When a 30s Au NPs deposit is applied (TiO_2/Au (0.5)/CdS), a small reduction in the photocurrent is obtained (J_{sc} 9.5 mA) maintaining relatively constant for longer deposition times (9.5 and 9.4 mA for 2.5 and 7.5 min respectively). At the same time, the Au NPs deposit increases the V_{oc} to 612 mV at 30 seconds of deposit. Maintaining almost constant for 2.5 min of deposit (618 mV) and reducing for higher times (570 mV for 7.5 min). In a similar way, the Au NPs deposit increases the FF to 51.0% with the first 30 seconds of electrophoresis, and maintaining almost constant for higher deposition times (50 and 50.3% for 2.5 and 7.5 min respectively). Finally, to test the deposition order effect, TiO_2/CdS/Au samples were made. Inset in Fig. 4 shows the champion cells of each configuration (TiO_2/CdS,TiO_2/CdS/Au and TiO_2/Au/CdS). It can be seen that Au NPs addition after CdS sensitization result in a general reduction of the cell performance, possibly due to a partial removing or damage of the QDs.

3.2.2. IPCE Characterization

J_{sc} is mainly dominated by two phenomena, the photogeneration (i.e. the process where photons are absorbed to generate electron hole pairs) and the injection (the transference of the electrons and holes from the photogenerator to the electron and hole transporter respectively). To understand the photogeneration in terms of the contribution of each wavelength, the incident photon to current conversion efficiency (IPCE), A.K.A.external quantum efficiency (QE),

Table 1
Characteristic Short circuit current, open circuit voltage, Fill Factor and photo-conversion efficiencies of Au decorated TiO_2/CdS films under one sun illumination.

Sample	J_{sc} mA/cm^2	V_{oc} mV	FF%	η %
TiO_2/CdS(7)/ZnS	9.85	-575	46.52	2.63
TiO_2/Au(0.5)/CdS(7)/ZnS	9.48	-612	51.04	2.96
TiO_2/Au(2.5)/CdS(7)/ZnS	9.53	−618	50.06	2.95
TiO_2/Au(7.5)/CdS(7)/ZnS	9.44	−570	50.37	2.71

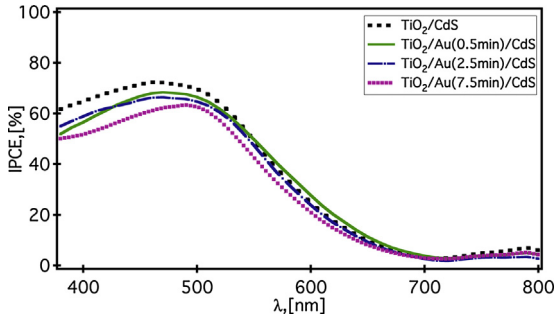

Fig. 5. Representative IPCE curves of CdS QDs sensitized solar cells decorated by electrophoretic deposition with Au NPs.

was calculated by was calculated by the expression.

$$IPCE(\%) = \frac{1240 x J_{sc}(mA/cm^2)}{\lambda(nm) x P_{inc}(mW/cm^2)} x100, \quad (3)$$

Where P_{inc} stand for the light incident power. Fig. 5 shows the IPCE curves TiO2/Au/CdS samples. Here it can be appreciated that samples without Au NPs have a QE higher than 60% in the 380-530 nm, reaching it maximum at 460 nm (QE = 72%) and rapidly decreasing for λ>550 nm.With 0.5 min of Au NPs deposit (green line) a reduction in the QE in the 380-530 nm region is obtained with an small increase over a wide range of wavelengths between 550 and 700 nm, when the deposition time is increased to 2.5 min (blue line) it is obtained almost the same spectrum than for 0.5 min but without the contribution in the 550 to 700 nm. With higher deposition times (7.5 min, pink line) a stronger reduction of QE are observed. These reductions in the QE are consistent with the reductions in Jsc. These results in conjunction with the absorbance curves indicate that a small coverage with Au NPs could increase the photoabsorption of the CdS or electron injection into the mesoscopic TiO_2 due to the good conductivity of Au NPs. While for higher coverage Au NPs act as an optical filter reducing the amount of light reaching the absorbing elements (TiO_2 and QDs).

3.2.3. Electrochemical Impedance

Electrochemical impedance spectroscopy (EIS) measurements were carried out to explain the trends observed in the solar cell parameters (particularly V_{oc} and FF) in terms of the internal physical processes when Au Nanoparticles are deposited. To do appropriate fit the EIS measurements, the equivalent circuit shown in Fig. 6 was used [51–55] Where R_s is the series resistance and is related to the resistance of FTO and the wires resistance, R_{con} and C_{con} are the resistance and capacitance associated to the charge transfer in the counter electrode, R_t (=r_t/L) is the transport resistance, and is related with the resistance to the electron flux inside of TiO_2/sensitizer composite, which include the electron transport inside of the nanostructured particles, and between the nanostructured particles. R_{rec} (=r_{rec}/L) and C_μ (=c_μL) are the charge transfer resistance and the chemical capacitance respectively. Where R_{rec} is inversely proportional to the recombination rate. These last three mentioned elements are denoted in lowercase letters in Fig. 6 meaning the element per unit length for a film of thickness L, because they are distributed in a repetitive arrangement of a transmission line. All fitted circuit values, adjust the experimental curves with a relative error of 5% or lower.

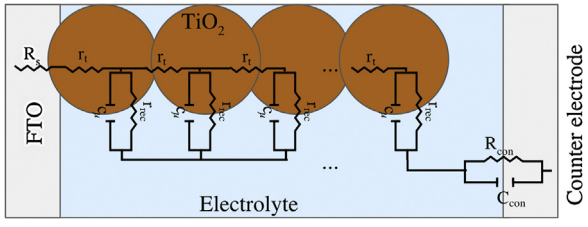

Fig. 6. Schematic representation of the equivalent circuit used to fit the impedance measurements, showing the principal components of the film region where the correspondent physical process occurs: the series resistance, R_s; the transport resistance, R_t; the recombination resistance, R_{rec}; the chemical capacitance C_μ; The charge transfer an capacitance at the counter electrode R_{con} and C_{con}.

C_μ, R_{rec} and R_t extracted from the EIS fitting of the CdS and Au/CdS sensitized solar cells are shown in Fig. 7. Cμ is represented versus the applied voltage (V_{app}) less the voltage drop due to FTO and wire resistance at the photoanode ($V_{series} = R_s$xJ). Then the new voltage is defined as $V_f = V_{app}$-V_{series} [51,56,57]. The chemical capacitance is proportional to the density of states (DOS) in the band gap, DOS increases exponentially with the proximity to the conduction band (CB), then, an increase in C_μ suggest a displacement to lower energies of the TiO_2 CB. R_{rec} and R_t are

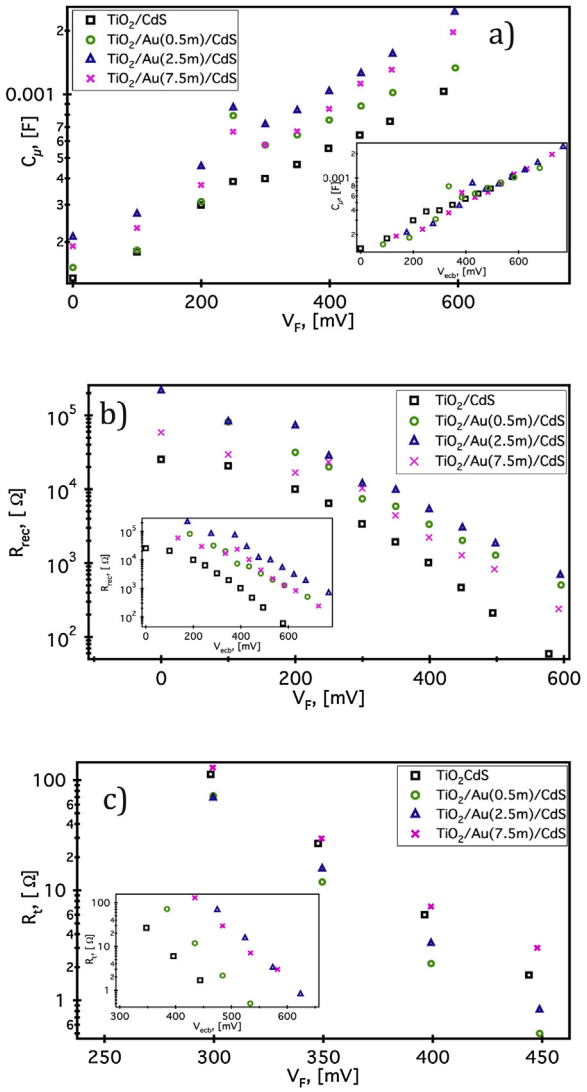

Fig. 7. Impedance spectroscopy characterization of the TiO_2/Au/CdS(S)/ZnS(S) cells at 0.5, 2.5 and 7.5 min of Au NPs deposit, showing: a) Chemical capacitance, Cμ in the V_f representation and V_{ecb} representation in the inset. b) Recombination resistance, R_{rec}, also in both representations. c) Transport resistance R_t as function of Final votage V_f and inset R_t as a function of voltage equivalent conduction band V_{ecb}.

exponentially dependent on carrier density (i.e. the distance to CB), then, to correctly evaluate this parameters a new potential is defined where, the measurements are at the same equivalent value of position to the CB of each device, using the equation [24,57].

$$V_{ecb} = V_F - \Delta V_i, \quad (4)$$

Where ecb means equivalent conduction band and ΔV_i is the voltage shift observed between the Au decorated samples and the CdS sensitized film in Fig. 7 a. After the voltage correction Cμ overlaps as shown in the inset of Fig. 7 comparing R_{rec} and C_μ for the cells, it is viable to understand the origin in the V_{oc} variation. [21,25,34,35,51]. Higher V_{oc} observed in Au decorated cells could be due to three processes: (1) An increase in the absorption. (2) A shift in the TiO_2 CB, and/or (3) a change in the recombination rate. An increase in the photo absorption will result in an increase in J_{sc} and V_{oc}. As previously discussed the photoabsorption in these samples is reduced. Then, hypothesis 1 can be discarded

The second effect, a shift in the TiO_2 CB, produces a movement of the TiO_2 electron quasi-Fermi level, which determines the V_{oc}, then an upward of the TiO_2 CB will mean an increase in the V_{oc}. This upward displacement of the conduction band is identified, by a shift to higher potentials of C_μ (i.e. a reduction of the capacitance). When Au are deposited, a general increase in Cμ is observed (see Fig. 7 a) which means a downshift in the conduction band and the V_{oc}. It is observed that for short depositions times (0.5 min) a downshift of about 85 mV is obtained (green circles), when the deposition time is increased to 2.5 min the band shift increases to approximately 175 mV (blue triangles). Finally, for higher deposition times, a reduction in the shift is obtained (135 mV at 7.5 min). These results as the obtained for J_{sc} contravene the observed V_{oc} behavior of such samples, indicating that the photocurrent is not the dominant process in the V_{oc} variations.

The third effect, the recombination rate, can be also determined with EIS by analyzing the R_{rec}. Where an increase in this parameter indicates a reduction in the electron recombination processes from the TiO_2 CB to acceptor states either in the electrolyte or the sensitizer [36,57]. Comparing TiO_2/Au/CdS and TiO_2/CdS samples in Fig. 7b, it is observed that with 0.5 min of deposit R_{rec} increases (green circles), indicating an increase of the V_{oc}. When the deposition time is increased to 2.5 min a higher increase in R_{rec} is obtained (blue triangles). If the deposition time still increasing (7.5 min) R_{rec} have a small reduction, resulting in a resistance a little lower than the obtained for the samples with 0.5 min of deposit. Analyzing these same results in the V_{ecb} convention, it is observed that with the first 30 seconds of Au NPs deposit the increase in R_{rec} is stronger than the observed in the V_f convention, and when the deposition time is increased to 2.5 min still increasing, while for 7.5 min of Au NPs deposit R_{rec} drops until reach the resistance obtained for 0.5 min of deposit. These results imply that the observed increases in R_{rec} in the V_f convention are the result of strong reductions in the recombination processes (possibly due to a passivation of the TiO_2 superficial defects) that are slightly masked by the TiO_2's CB displacement.

Then, when Au NPs are deposited, two simultaneous processes affect the V_{oc}. On one side the TiO_2 CB is downshifted reducing the V_{oc}, but at the same time Recombination processes are considerably reduced upshifting the Fermi level and the V_{oc}. At the end the reduction of recombination processes overcome the effect of the CB shift increasing the photovoltage.

Another important parameter that is positively affected by the Au deposit is the FF. Variations in this parameter can be due to changes in the Transport resistance (R_t), where a reduction in R_t results in a FF increment [12,15,18–21,51]. The R_t behavior in the samples (Fig. 7 c) indicate that for 30 seconds of Au NPs deposit (green circles) slightly reduces R_t, with the increase in the deposition time R_t increases until the 7.5 minutes deposit, when R_t reaches the same level than samples without Au NPs deposit indicating an increase in the electron transport (and the FF) with the first 30s of Au NPs deposit and an slow reduction of these parameter with higher deposition times, which match with the behavior observed in Table 1. Analyzing these curves in the V_{ecb} convention (inset of Fig. 7 c) it could be appreciated than the Au deposit increases the resistance to the electron flux, this suggest that Au NPs pore filling is hindering the movement of the electrolyte ions affecting the electron motion in the TiO_2. However, the CB shift produces an effective increase in the electron flux that overcompensates the Au NPs pore filling effect resulting in the increase of the FF.

4. Discussion

In summary, when a photon of visible light (λ = 370-570 nm) insides on the CdS QDs of TiO_2/CdS samples, an electron hole pair is generated (see Fig. 8 a), the electron is injected from the CdS QD's CB to the TiO_2's CB driven by the energy difference between the bands Δc, then it will be transported by the TiO_2 and in an ideal case to the FTO and the electrical circuit. However, some electrons interact whit trap levels in the QD/TiO_2, giving a recombination process (red arrow in Fig. 8 a) reducing the performance of the cell. In the other side, holes are taken by the electrolyte via the oxidation of the S^{2-}_{x-1} ions, as shown in Fig. 8a. After that, the resulting S^{2-}_{x} ions moved by diffusion to the counter electrode where they are reduced to S^{2-}_{x-1} ions and the circuit is closed. As previously discussed, in these conditions J_{sc} is principally determined by the photogeneration process (the amount of photons that inside in the QDs and the efficiency to convert such photons in electron hole pairs), and the injection process (driven by Δχ). Meanwhile, the V_{oc} is due to the energy difference between the Fermi level of the TiO_2 (E_F) and the redox level. Finally, the FF

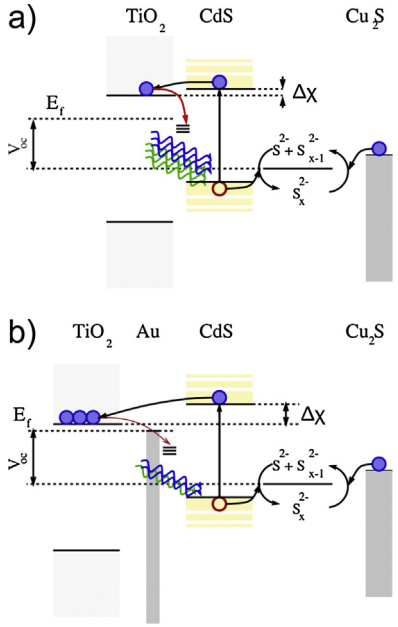

Fig. 8. Schematic representation of the energy levels distribution for: a) TiO_2/CdS cells and b) TiO_2/Au/CdS cells, showing the electron and hole flux (blue and red circles respectively), the energy difference between the TiO_2's CB and the CdS QD's CB, Δχ, the TiO_2's quasi-Fermi level E_F and the open circuit voltage V_{oc}.

will be determined by the ratio of the transport and recombination processes.

When Au NPs are deposited various simultaneous processes occurred (Fig. 8 b). (1) Au NPs act as an optical filter, reducing the amount of light that reaches the CdS QDs, which will result in a reduction of J_{sc}. (2) The TiO_2 CB is downshifted by the energy levels equilibration process. This band movement will affect at the same time three parameters, J_{sc} is slightly increased by the increase in the potential energy between the sensitizer and the TiO_2 ($\Delta\chi$), V_{oc} is reduced by the downshift of E_F, and the FF is considerable increased by a reduction in the transport resistance. (3) The recombination processes are considerably reduced, resulting in higher amount of electrons in the TiO_2's CB; this upshifts E_F and increments V_{oc}. Then, when these three processes are combined in the right proportion what is obtained is a reduction in J_{sc}, an increase in V_{oc} and an increase in FF that together give an increase in the photoconversion efficiency from 2.6 to 2.9%.

5. Conclusions

The photovoltaic properties of CdS QD-sensitized TiO_2 NC films decorated by electrophoresis with Au NPs at different deposition times have been systematically studied and analyzed. It was demonstrated that Au NPs could improve the photoconversion efficiency of TiO_2/CdS QDs films when applied very short deposition times (30 seconds), by increasing V_{oc} and FF sacrificing J_{sc}. IPCE measurements show that the presence of Au NPs reduces the capacity of the CdS QDs to absorb light, and impedance spectroscopy analyses indicates that Au NPs at the same time moves down the TiO_2's CB and reduces the recombination processes. The band movement helps to reduce the photocurrent losses due to the absorption issue, and the reduction in the recombination processes give the observed increase in V_{oc} (from 575 to 611 mV) and FF (from 46 to 50%), that result in the final increase in η from 2.6 to 2.9%.

Acknowledgments

We acknowledge financial support from CONACYT through grant 134111, the UC-MEXUS program grant 00007, the European Community Seven Framework Program (FP7- 428 NMP-2010-EU-MEXICO), CIO-UGTO 2013–2015 and the CEMIE-Solar (04002) consortium. D. Esparza, and A. Ceja acknowledge scholarship from CONACYT and thanks to Maria Christian Albor for SEM and EDS analysis. Isaac Zarazúa thanks to CONACYT for the postdoctoral fellow.

References

[1] P.V. Kamat, Meeting the clean energy demand: nanostructure architectures for solar energy conversion, J. Phys. Chem. C 111 (2007) 2834–2860.
[2] T. Soga, Nanostructured Materials for Solar Energy Conversion, Elsevier, Burlington, MA, 2007.
[3] M.K. Hubbert, Energy from fossil fuels, Scince 109 (1949) 103–109.
[4] B. Gregg, Excitonic solar cells, J. Phys. Chem. B 107 (2003) 4688–4698.
[5] M.K. Hubbert, The world's evolving energy system, American Journal of Physics 49 (1981) 1007–1029.
[6] C.D. Lokhande, B.-O. Park, H.-S. Park, K.-D. Jung, O.-S. Joo, Electrodeposition of TiO2 and RuO2 thin films for morphology-dependent applications, Ultramicroscopy 105 (2005) 267–274, doi:http://dx.doi.org/10.1016/j.ultramic.2005.06.048.
[7] G.P. Smestad, S. Spiekermann, J. Kowalik, C.D. Grant, A.M. Schwartzberg, J. Zhang, et al., A technique to compare polythiophene solid-state dye sensitized TiO2 solar cells to liquid junction devices, Sol. Energy Mater. Sol. Cells 76 (2003) 85–105, doi:http://dx.doi.org/10.1016/s0927-0248(02) 00252-0.
[8] M.A. Green, K. Emery, Y. Hishikawa, W. Warta, E.D. Dunlop, Solar cell efficiency tables (Version 45), Prog. Photovolt: Res. Appl. 23 (2015) 1–9, doi:http://dx.doi.org/10.1002/pip.2573.
[9] R. Beranek, H. Tsuchiya, T. Sugishima, J. Macak, L. Taveira, S. Fujimoto, et al., Enhancement and limits of the photoelectrochemical response from anodic TiO2 nanotubes, Appl. Phys. Lett. 87 (2005) 243114.
[10] G.K. Mor, K. Shankar, M. Paulose, O.K. Varghese, C.A. Grimes, Use of Highly-Ordered TiO2 Nanotube. Arrays in Dye-Sensitized Solar Cells, Nano. Lett. 6 (2005) 215–218.
[11] T. Chou, Q. Zhang, B. Russo, Titania Particle Size Effect on the Overall Performance of Dye-Sensitized Solar Cells, J. Phys. Chem. C 111 (2007) 6296–6302.
[12] A. Kongkanand, K. Tvrdy, K. Takechi, M. Kuno, P.V. Kamat, Quantum Dot Solar Cells. Tuning Photoresponse through Size and Shape Control of CdSe-TiO2 Architecture, J. Am. Chem. Soc. 130 (2008) 4007–4015.
[13] B. O'regan, M. Grätzel, A low-cost, high-efficiency solar cell based on dye-sensitized colloidal Ti02 films, Nature 353 (1991) 737–740.
[14] P. Liska, K. Thampi, M. Gratzel, Nanocrystalline dye-sensitized solar cell/copper indium gallium selenide thin-film tandem showing greater than 15% conversion efficiency, Appl. Phys. Lett. 88 (2009) 203103.
[15] I. Mora-Seró, T. Dittrich, A. Susha, A. Rogach, J. Bisquert, Large improvement of electron extraction from CdSe quantum dots into a TiO2 thin layer by N3 dye coabsorption, Thin Solid Films 516 (2008) 6994–6998.
[16] Y. Chiba, A. Islam, Y. Watanabe, R. Komiya, Dye-sensitized solar cells with conversion efficiency of 11.1%, J. J. Appl. Phys. 45 (2006) L638–L640.
[17] K. Hara, T. Horiguchi, T. Kinoshita, K. Sayama, Highly efficient photon-to-electron conversion with mercurochrome-sensitized nanoporous oxide semiconductor solar cells, Sol. Energy Mater. Sol. Cells 64 (2000) 115–134.
[18] I. Robel, V. Subramanian, M. Kuno, P.V. Kamat, Quantum dot solar cells. Harvesting light energy with CdSe nanocrystals molecularly linked to mesoscopic TiO2 films, J. Am. Chem. Soc. 128 (2006) 2385–2393.
[19] T. Lopez-Luke, A. Wolcott, L. Xu, S. Chen, Z. Wen, J. Li, et al., Nitrogen-doped and CdSe quantum-dot-sensitized nanocrystalline TiO2 films for solar energy conversion applications, J. Phys. Chem. C 112 (2008) 1282–1292.
[20] A. Franceschetti, J. An, A. Zunger, Impact ionization can explain carrier multiplication in PbSe quantum dots, Nano. Lett. 6 (2006) 2191–2195.
[21] I. Zarazúa, E. De La Rosa, T. Lopez-Luke, J. Reyes-Gomez, S. Ruiz, C. Angeles Chavez, et al., Photovoltaic Conversion Enhancement of CdSe Quantum Dot-Sensitized TiO2 Decorated with Au Nanoparticles and P3OT, J. Phys. Chem. C. 115 (2011) 23209–23220.
[22] C.-F. Chi, H.-W. Cho, H. Teng, C.-Y. Chuang, Y.-M. Chang, Y.-J. Hsu, et al., Energy level alignment, electron injection, and charge recombination characteristics in CdS/CdSe cosensitized TiO[sub 2] photoelectrode, Appl. Phys. Lett. 98 (2011) 012101, doi:http://dx.doi.org/10.1063/1.3533642.
[23] D.A. Hines, P.V. Kamat, Quantum Dot Surface Chemistry: Ligand Effects and Electron Transfer Reactions, J. Phys. Chem. C 117 (2013) 14418–14426, doi:http://dx.doi.org/10.1021/jp404031s.
[24] L. Liu, G. Wang, Y. Li, Y. Li, J.Z. Zhang, CdSe quantum dot-sensitized Au/TiO2 hybrid mesoporous films and their enhanced photoelectrochemical performance, Nano Research (2011) 1–10.
[25] N. Chandrasekharan, P.V. Kamat, Improving the Photoelectrochemical Performance of Nanostructured TiO2 Films by Adsorption of Gold Nanoparticles†, J. Phys. Chem. B. 104 (2000) 10851.
[26] Y. Tian, T. Tatsuma, Mechanisms and Applications of Plasmon-Induced Charge Separation at TiO2 Films Loaded with Gold Nanoparticles, J. Am. Chem. Soc 127 (2005) 7632–7637, doi:http://dx.doi.org/10.1021/ja042192u.
[27] M. Mingkui Wang, High-Performance Liquid and Solid Dye-Sensitized Solar Cells Based on a Novel Metal-Free Organic Sensitizer, Adv. Mater 20 (2008) 4460–4463.
[28] M. Antoniadou, E. Stathatos, N. Boukos, A. Stefopoulos, Study of hybrid solar cells made of multilayer nanocrystalline titania and poly (3-octylthiophene) or poly-(3-(2-methylhex-2-yl)-oxy- carbonyldithiophene), Nanotech. 20 (2009) 495201.
[29] D.M. Schaadt, B. Feng, E.T. Yu, Enhanced semiconductor optical absorption via surface plasmon excitation in metal nanoparticles, Appl. Phys. Lett. 86 (2005) 063106-063106-3. 10.1063/1.1855423.
[30] S. Pillai, K.R. Catchpole, T. Trupke, G. Zhang, J. Zhao, M.A. Green, Enhanced emission from Si-based light-emitting diodes using surface plasmons, Appl. Phys. Lett. 88 (2006) 161102, doi:http://dx.doi.org/10.1063/1.2195695.
[31] D. Derkacs, S. Lim, P. Matheu, W. Mar, Improved performance of amorphous silicon solar cells via scattering from surface plasmon polaritons in nearby metallic nanoparticles, Appl. Phys. Lett. (2006) .
[32] S. Pillai, K. Catchpole, T. Trupke, Surface plasmon enhanced silicon solar cells, J. Appl. Phys. (2007) .
[33] H.R. Stuart, D.G. Hall, Island size effects in nanoparticle-enhanced photodetectors, Appl. Phys. Lett. 73 (1998) 3815–3817, doi:http://dx.doi.org/10.1063/1.122903.
[34] V. Subramanian, E. Wolf, P.V. Kamat, Semiconductor-Metal Composite Nanostructures. To What Extent Do Metal Nanoparticles Improve the Photocatalytic Activity of TiO2 Films? J. Phys. Chem. B 105 (2001) 11439–11446.
[35] I. Zarazúa, T. Lopez-Luke, J. Reyes-Gomez, A. Torres Castro, J.Z. Zhang, E. De la Rosa, Impedance Analysis of CdSe Quantum Dot-Sensitized TiO2 Solar Cells Decorated with Au Nanoparticles and P3OT, Journal of The Electrochemical Society (2014) .
[36] G. Burgeth, H. Kisch, Photocatalytic and photoelectrochemical properties of titania-chloroplatinate(IV), Coordination Chemistry Reviews 230 (2002) 41–47, doi:http://dx.doi.org/10.1016/s0010-8545(02) 00095-4.
[37] Y. Tian, Plasmon-Induced Photoelectrochemistry at Metal Nanoparticles Supported on Nanoporous TiO2W, Chem. Comm. (2004) .
[38] D. Esparza, I. Zarazúa, T. Lopez-Luke, R. Carriles, Photovoltaic Properties of Bi2S3 and CdS Quantum Dot Sensitized TiO2 Solar Cells, Electrochimical Acta (2015) 486–492.

[39] A. Cerdán-Pasarán, T. Lopez-luke, D. Esparza, I. Zarazúa, E. De la Rosa, R. Fuentes-Ramírez, et al., Photovoltaic properties of multilayered quantum dot/quantum rod-sensitized TiO 2solar cells fabricated by SILAR and electrophoresis, Phys. Chem. Chem. Phys. 17 (2015) 18590–18599, doi:http://dx.doi.org/10.1039/C5CP02541A.
[40] D. Esparza, I. Zarazúa, T. Lopez-luke, A. Cerdán-Pasarán, A. Sánchez-Solís, A. Torres-Castro, et al., Effect of Different Sensitization Technique on the Photoconversion Efficiency of CdS Quantum Dot and CdSe Quantum Rod Sensitized TiO 2Solar Cells, J. Phys. Chem. C. 119 (2015) 13394–13403, doi:http://dx.doi.org/10.1021/acs.jpcc.5b01525.
[41] V. González-Pedro, C. Sima, G. Marzari, P.P. Boix, S. Giménez, Q. Shen, et al., High performance PbS Quantum Dot Sensitized Solar Cells exceeding 4% efficiency: the role of metal precursors in the electron injection and charge separation, Phys. Chem. Chem. Phys. 15 (2013) 13835, doi:http://dx.doi.org/10.1039/c3cp51651b.
[42] I. Mora-Sero, S. Giménez, F. Fabregat-Santiago, R. Gomez, Q. Shen, T. Toyoda, et al., Recombination in Quantum Dot Sensitized Solar Cells, Acc. Chem. Res. 42 (2009) 1848–1857, doi:http://dx.doi.org/10.1021/ar900134d.
[43] N. Guijarro, J.M. Campiña, Q. Shen, T. Toyoda, T. Lana-Villarreal, R. Gomez, Uncovering the role of the ZnS treatment in the performance of quantum dot sensitized solar cells, Phys. Chem. Chem. Phys. 13 (2011) 12024, doi:http://dx.doi.org/10.1039/c1cp20290a.
[44] C. Chuang, P.R. Brown, V. Bulović, M.G. Bawendi, Improved performance and stability in quantum dot solar cells through band alignment engineering: Nature Materials: Nature Publishing Group, Nature Mater. (2014) .
[45] Y. Nakato, M. Shioji, H. Tsubomura, Photoeffects on the potentials of thin metal films on a n-TiO2 crystal wafer. The mechanism of semiconductor photocatalysts, Chem. Phys. Lett. 90 (1982) 453–456, doi:http://dx.doi.org/10.1016/0009-2614(82) 80253-4.
[46] J. Nelson, The physics of solar cells, Imperial college press, 2003.
[47] N. Parsi Benehkohal, V. González-Pedro, P.P. Boix, S. Chavhan, R. Tena-Zaera, G. P. Demopoulos, et al., Colloidal PbS and PbSeS Quantum Dot Sensitized Solar Cells Prepared by Electrophoretic Deposition, J. Phys. Chem. C 116 (2012) 16391–16397, doi:http://dx.doi.org/10.1021/jp3056009.
[48] P.P. Mahmoud Samadpour, S.G. Boix, A. imenez, I. zam, Z. raji, N. ad, T. ima, I. aghavinia, M. van, ora-S, ero et al, Fluorine Treatment of TiO2 for Enhancing Quantum Dot Sensitized Solar Cell Performance, J. Phys. Chem. C 115 (2011) 14400–14407, doi:http://dx.doi.org/10.1021/jp202819y.
[49] A. Braga, S. Giménez, I. Concina, A. Vomiero, I. Mora-Sero, Panchromatic Sensitized Solar Cells Based on Metal Sulfide Quantum Dots Grown Directly on Nanostructured TiO2 Electrodes, The Journal of Physical Chemistry Letters. 2 (2011) 454–460, doi:http://dx.doi.org/10.1021/jz2000112.
[50] M. Solis de la Fuente, R.S. Sanchez, V. González-Pedro, P.P. Boix, S.G. Mhaisalkar, M.E. Rincón, et al., Effect of Organic and Inorganic Passivation in Quantum-Dot-Sensitized Solar Cells, The Journal of Physical Chemistry Letters 4 (2013) 1519–1525, doi:http://dx.doi.org/10.1021/jz400626r.
[51] S. Giménez, T. Lana-Villarreal, R. Gomez, S. Agouram, V. Muñoz-Sanjosé, I. Mora-Sero, Determination of limiting factors of photovoltaic efficiency in quantum dot sensitized solar cells: Correlation between cell performance and structural properties, J. Appl. Phys. 108 (2010) 064310, doi:http://dx.doi.org/10.1063/1.3477194.
[52] J. Bisquert, Theory of the Impedance of Electron Diffusion and Recombination in a Thin Layer, J. Phys. Chem. B 106 (2002) 325–333, doi:http://dx.doi.org/10.1021/jp011941g.
[53] P.N. Kumar, R. Narayanan, M. Deepa, A.K. Srivastava, Au@poly(acrylic acid) plasmons and C60 improve the light harvesting capability of a TiO2/CdS/CdSeS photoanode, J. Mater. Chem. A 2 (2014) 9771, doi:http://dx.doi.org/10.1039/c4ta01140f.
[54] F. Fabregat-Santiago, J. Bisquert, G. Garcia-Belmonte, G. Boschloo, A. Hagfeldt, Influence of electrolyte in transport and recombination in dye-sensitized solar cells studied by impedance spectroscopy, Sol. Energy Mater. Sol. Cells 87 (2005) 117–131, doi:http://dx.doi.org/10.1016/j.solmat.2004.07.017.
[55] Q. Wang, S. Ito, M. Grätzel, F. Fabregat-Santiago, I. Mora-Sero, J. Bisquert, et al., Characteristics of High Efficiency Dye-Sensitized Solar Cells, J. Phys. Chem. B 110 (2006) 25210–25221, doi:http://dx.doi.org/10.1021/jp064256o.
[56] V. González-Pedro, X. Xu, I. Mora-Sero, J. Bisquert, Modeling High-Efficiency Quantum Dot Sensitized Solar Cells, ACS Nano 4 (2010) 5783–5790, doi:http://dx.doi.org/10.1021/nn101534y.
[57] F. Fabregat-Santiago, G. Garcia-Belmonte, I. Mora-Sero, J. Bisquert, Characterization of nanostructured hybrid and organic solar cells by impedance spectroscopy, Phys. Chem. Chem. Phys. 13 (2011) 9083, doi:http://dx.doi.org/10.1039/c0cp02249g.